Field Measurement and Analysis of an Electric Bus Charging Station: A Case Study on Transformer Losses and Harmonic Impacts

G. Y. Li and G. W. Chang*
Department of Electrical Engineering
National Chung Cheng University
Chia-Yi, Taiwan ROC
*garywkchang@gmail.com

H. J. Lu
Green Energy and Environment Research Laboratories
Industrial Technology Research Institute
Hsin-Chu, Taiwan ROC
lhengjiu@gmail.com

***Abstract*—The electrification of public transportation requires large-scale, high-power electric vehicle (EV) charging stations, which introduce significant power quality challenges. A primary concern is the impact of harmonic currents, generated by power electronic converters, on the thermal stress and operational losses of distribution transformers. This paper addresses the scarcity of long-term field assessments in the literature by presenting case studies based on field measurements at a commercial electric bus charging station. This study assesses data collected simultaneously from the primary and secondary sides of a 2000 kVA distribution transformer. This study also distinguishes genuine power quality threats from misleading harmonic distortion artifacts observed at low loads. Results reveal that during the charging phases, the harmonic loss factor for winding eddy currents stabilized within a range of 10 to 30. This finding empirically confirms that non-sinusoidal currents from EV charging profiles increase operational losses, underscoring the necessity of applying harmonic derating factors for reliable asset management and future infrastructure design.**

***Index Terms*—Electric bus charging stations, distribution transformers, harmonic distortion, transformer losses.**

I. Introduction

The electrification of public transportation has emerged as a pivotal strategy in the global effort to reduce greenhouse gas emissions, improve urban air quality, and advance sustainable mobility. In the transition from conventional diesel-powered fleets to battery electric vehicles (EVs), high-power charging stations have become a critical component of this transformation [1]. However, the integration of large-scale EV charging stations into existing power distribution networks introduces a new set of power quality challenges [2], [3]. These challenges can lead to transformer and line overloads, voltage deviations, and degradation of power quality indices, such as the total harmonic distortion (THD) [4], [5].

The use of power electronic converters in EV chargers introduces significant harmonic currents into the grid, which can propagate through the distribution system and affect voltage profiles, increase losses, and stress sensitive equipment [6]. Studies have shown that high concentrations of EV charging stations, especially when clustered or operating simultaneously, can exacerbate these issues. As a result, the limits set by standards, such as IEEE Std. 519, are exceeded under practical operating scenarios [7].

Among the grid components most vulnerable to the impacts of EV charging are distribution transformers. These assets are not only the most costly components but are also critical for reliable power delivery. According to IEEE Std. C57.110, harmonics increase transformer losses through additional eddy current and stray flux losses in the windings and core, leading to abnormal temperature rise [8]. Recent studies based on IEEE Std. C57.110 have validated that even moderate levels of harmonic distortion can cause significant derating in transformers. Furthermore, the cumulative effect of harmonics and overloading can reduce the kVA rating of transformers, increase operational losses, and compromise the reliability of the entire distribution system [9], [10]. Advanced modeling and field measurements have shown that coordinated charging strategies, harmonic filtering, and real-time transformer monitoring are essential to mitigate these risks.

While some studies have utilized simulations and analytical models to estimate the potential impacts of EV integration, this paper presents empirical data from long-term field measurements of real-world, commercial-scale EV charging operations. This paper aims to address this impact by presenting a comprehensive case study of a 2000 kVA distribution transformer serving an electric bus charging station. By combining extensive on-site measurements with the application of the IEEE Std. C57.110, this study seeks to analyze the transformer's total losses and provide critical insights.

The rest of the paper is organized as follows. Section II details the system architecture of the electric bus charging station and the field measurement methodology employed. Section III analyzes the site's operational load profile and outlines the theoretical framework for transformer loss calculation, including the methodology from IEEE Std. C57.110. Section IV presents the detailed case study results. Finally, Section V draws the main conclusions from this study.

979-8-3315-8138-1

II. System Description and Measurement Methodology

The measurements for this study were conducted at an electric bus charging station located in Taipei, Taiwan. This facility serves a fleet of commercial electric buses. Its concentrated load profile and structured operational schedule make it a valuable environment for investigating the power quality impacts and transformer performance associated with EV fleet charging.

A. Electrical System Architecture

The charging station is supplied directly from a 22.8 kV medium-voltage distribution feeder. The electrical architecture within the facility is straightforward and representative of similar installations. As depicted in the conceptual single-line diagram in Fig. 1, a single oil-immersed transformer steps down the supply to a low-voltage level of 380/220 V. This low-voltage supply is then distributed through a main switchboard to the charging infrastructure and other auxiliary site loads.

The charging infrastructure consists of thirteen fast-charging stations, each with a nominal power rating of 120 kW. This configuration results in a total installed charger capacity of 1560 kW. Table I lists the nameplate data and key operational parameters of the 2000 kVA distribution transformer. Table II presents the specifications of the charging units.

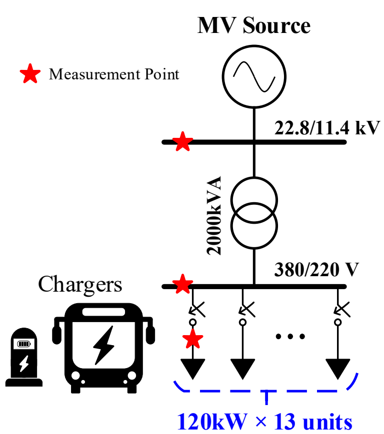

Figure 1. Architecture of the electric bus charging station.

TABLE I. Distribution Transformer Specifications.

Type	Oil immersed
Capacity (kVA)	2000
Primary (kV)	22.8/11.4
Secondary (kV)	0.38/0.22
Impedance (%)	5.5 – 6.5
No-load Current (%)	2.5
Full-Load Loss (kW)	26.342
Voltage Regulation (%)	1.3
Efficiency (%)	98.7

TABLE II. Charging Unit Specifications.

Charging Coupler	CCS1/CCS2
Input Power	192A, 198kVA @400V 50Hz
Output Power	120kW
Input Voltage	380/400 Vac ±15%
DC Output Voltage	200 – 1000Vdc
Maximum Current	200A
Power Factor	≧0.99
Efficiency	≧94%

B. Measurement Methodology

The measurements were conducted over a month-long period, from July 23 to August 25, 2025. This extended duration was chosen to capture a full range of operational cycles, including weekdays, weekends, and varying load conditions. This consideration ensures the collected data is statistically representative of the typical operational behavior.

The instrumentation for this study consisted of HIOKI PQ3198 power quality analyzers, which were paired with HIOKI CT 7136 and 9694 current sensors. To build a comprehensive model of the system, monitoring points were strategically established to simultaneously record voltage and current at the primary and secondary sides of the distribution transformer, as well as at the input of a single charging unit. Recorded data was captured in two formats. First, high-resolution time-domain waveforms, each containing 16 consecutive cycles, were recorded every five minutes. Second, a set of true RMS-based power quality indices was logged at 3-second intervals. The IEEE Std. 519-2022 defines the aggregation window for very short time harmonics as a 3-second interval. [4].

III. Load Profile and Transformer Loss Analysis

A. Daily and Periodic Load Profile

The monthly measurement revealed a consistent and predictable operational pattern. Fig. 2 illustrates the active power demand of the station over a representative multi-day period, highlighting the clear weekly cycle. Fig. 3 provides a granular view of a typical 24-hour cycle. Analysis of these load profiles allows for the segmentation of the daily operation into four distinct phases:

- Daytime Charging (12:00 – 16:00): During this period, only a few buses undergo intermittent charging, resulting in low and fluctuating power.
- Grid Peak Avoidance (16:00 – 20:00): This phase corresponds to the local utility's peak demand period. To comply with requirements, all charging tasks are halted.
- Nightly Concentrated Charging (22:00 – 02:00): As the bus fleet returns from daily service, a coordinated charging session commences.
- Early Morning Standby (02:00 – 08:00): As vehicles reach their target state of charge, the load gradually tapers off, returning the system to a low-power standby state until the next operational cycle begins.

979-8-3315-8138-1

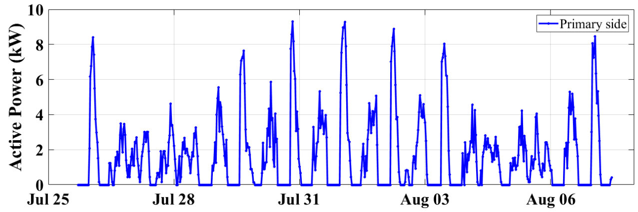

Figure 2. Representative active power demand over 12-day period.

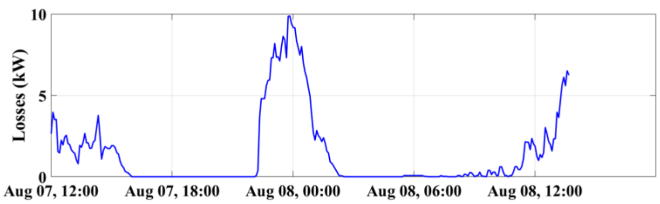

Figure 3. Typical 24-hour transformer losses.

B. Transformer Loading and Loss Analysis

The analysis of the transformer's performance under various operational scenarios is calculated based on the manufacturer's certified nameplate specifications provided in Table I. This procedure allows for the determination of total losses using the standard parameters. It should be noted that as the detailed internal design parameters are not available, this study relies exclusively on the standard electrical specifications provided in Table I for the subsequent analysis.

First, the operational stress on the transformer is quantified by its loading factor. This factor represents the ratio of the transformer's actual apparent load to its rated apparent power. For any given measured active power and associated power factor, the loading factor is determined by (1).

$$L = \frac{P_{\text{load}} / PF}{S_{rated}} \tag{1}$$

where P_{load} is the measured active power, PF is the power factor of the load, and S_{rated} is the rated apparent power.

The total loss of the transformer is fundamentally composed of two distinct components: the no-load loss and the load-dependent loss. The no-load loss, also known as core or iron loss, is considered constant whenever the transformer is energized. It can be computed from the nameplate specifications using the three-phase power equation, as expressed in (2).

$$P_{\text{NL}} = \sqrt{3} \times V_{\text{rated}} \times I_0 \times \cos\theta_0 \tag{2}$$

where V_{rated} is the rated line-to-line primary voltage, I_0 is the no-load current, and $\cos\theta_0$ is the no-load power factor, which is assumed to be 0.1 in this study.

Since the total loss is defined as the sum of the no-load loss and the rated load loss, the rated load loss can be determined by subtracting the calculated no-load loss from the manufacturer-specified full-load loss [8]. This relationship is presented in (3).

$$P_{\text{LL-R}} = P_{\text{Total-R}} - P_{\text{NL}} \tag{3}$$

where $P_{\text{Total-R}}$ stands for the rated total load loss provided in the transformer specification.

C. Theoretical Loss Calculation Considering Harmonics

To accurately quantify the additional thermal stress imposed by the non-sinusoidal currents drawn by EV chargers, this study employs the detailed loss decomposition model provided in IEEE Std. C57.110. This standard provides the definitive methodology for evaluating transformer capability when supplying harmonic-rich loads.

The fundamental principle of this standard is the separation of transformer load losses into three distinct components, as defined in (4).

$$P_{LL\text{-}R} = P_{\text{ohmic}} + P_{\text{EC}} + P_{\text{OSL}} \tag{4}$$

where P_{ohmic} is the basic ohmic loss in the windings that is proportional to the square of the current multiplied by the resistance. P_{EC} is the winding eddy-current loss, and P_{OSL} represents the other stray loss. When the transformer supplies a non-sinusoidal load, each of these loss components scales differently with the harmonic currents.

- P_{ohmic}: The loss is proportional to the square of the total RMS current. It is affected by all harmonic components equally.
- P_{EC}: This component is the primary cause of excessive harmonic heating. It is proportional not only to the square of the current but also approximately to the square of the harmonic frequency [11].
- P_{OSL}: These losses also increase with harmonics, but at a reduced rate. The standard estimates the frequency exponent as 0.8.

To quantify the aggregate impact of a measured harmonic spectrum on these components, the standard defines two key metrics. They are the harmonic loss factor for winding eddy currents and the harmonic loss factor for other stray losses, as expressed in (5) and (6).

$$F_{\text{HL}} = \sum_{h=1}^{h=h_{\max}} \left(\frac{I_h}{I_1}\right)^2 h^2 \Bigg/ \sum_{h=1}^{h=h_{\max}} \left(\frac{I_h}{I_1}\right)^2 \tag{5}$$

$$F_{\text{HL-STR}} = \sum_{h=1}^{h=h_{\max}} \left(\frac{I_h}{I_1}\right)^2 h^{0.8} \Bigg/ \sum_{h=1}^{h=h_{\max}} \left(\frac{I_h}{I_1}\right)^2 \tag{6}$$

where I_1 is the rms fundamental load current while I_h is the rms current at harmonic h.

Once the harmonic loss factors are established from the measured spectrum, it is critical to quantify how these non-sinusoidal conditions degrade the transformer's capability. The maximum permissible per-unit load current under a specific harmonic profile is determined by (7) [12].

$$I_{\max}(\text{pu}) = \sqrt{\frac{P_{LL-R}}{1 + (F_{\text{HL}} \times P_{\text{EC}}) + (F_{\text{HL-STR}} \times P_{\text{OSL}})}} \tag{7}$$

IV. Case Studies

This section presents a comprehensive analysis based on the field measurements collected from the 2000 kVA distribution transformer at the electric bus charging station. The analysis is divided into two parts. The first part presents the field measurement results and analysis. The second part details the harmonic loss calculation based on IEEE Std. C57.110.

A. Field Measurement Results and Analysis

The transformer's operational performance is evaluated by comparing the primary and secondary side active power. The difference between these two measurements represents the total transformer loss. As shown in Fig. 4, the measured losses show a distinct correlation with the load profile, peaking during the nightly concentrated charging phase.

To validate the accuracy of these measurements, a peak-load event from the data is analyzed. The field data shows a peak loss of 9.28 kW at a corresponding measured active power load of 925.8 kW. This load represents a loading factor of 0.463 pu relative to the 2000 kVA transformer rating. A theoretical total loss for this load point was then calculated using the nameplate values based on (1)-(3). The resulting theoretical loss of 9.57 kW shows a close alignment with the 9.28 kW measured value, representing a variance of only 3.1%. This small discrepancy confirms the baseline loss model.

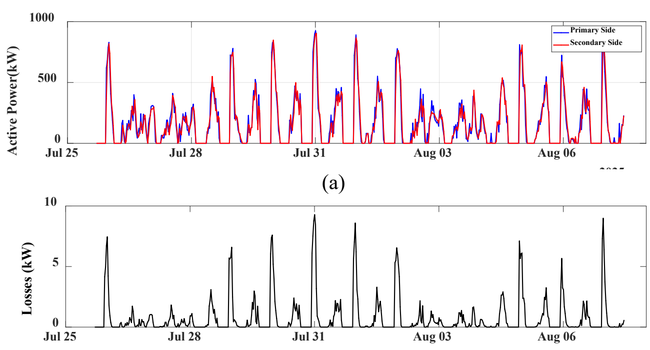

Figure 4. Time-series of (a) measured active power at the primary and secondary sides and (b) the resulting calculated transformer losses.

With the baseline model validated, the analysis proceeded to the power quality impact. As shown in Fig. 5, the total harmonic voltage distortion (THD_v) remains stable and well within acceptable limits. However, Fig. 6 indicates a critical aspect of analyzing variable-load environments: the total harmonic current distortion (THD_i) exhibits high volatility. This is because during intermittent charging phases, the fundamental current becomes small, inflating the THD_i metric to misleadingly high levels.

To provide a more accurate assessment, the total demand distortion (TDD) is adopted, which normalizes harmonics against the maximum demand load current. As shown in Fig. 7, the TDD remains significantly lower and more stable, providing a more practical representation of the harmonic impacts. In terms of pollution levels, the measured maximum TDD at the primary side is 5.38%, and the maximum THD_v is 2.01%. Given the short-circuit ratio and the voltage level, these values are well within the regulation limits based on IEEE Std. 519 [4].

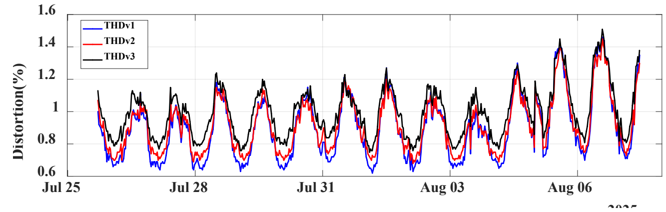

Figure 5. Measured total harmonic voltage distortion at the primary side for all three phases.

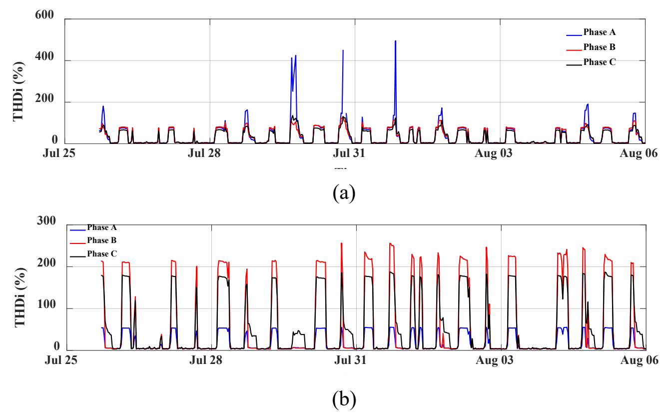

Figure 6. Measured total harmonic current distortion at (a) primary side and (b) secondary side for all three phases.

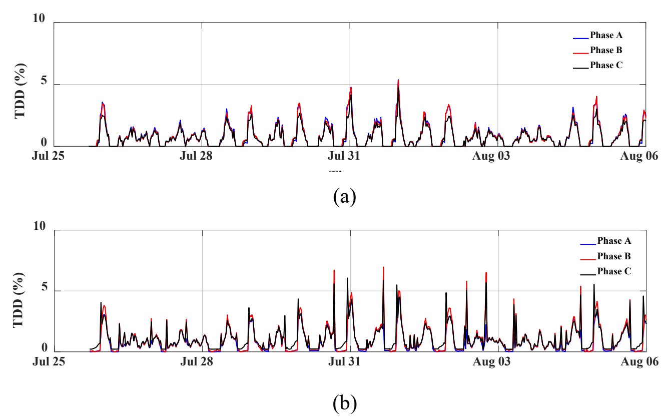

Figure 7. Measured total demand distortion at (a) primary side and (b) secondary side for all three phases.

B. Harmonic Loss Calculation Based on IEEE Std. C57.110

To quantify the impact of the harmonic currents observed in the previous subsection, IEEE C57.110 is applied. This requires the calculation of the harmonic loss factors from the measured harmonic spectrum. Figs. 8 and 9 illustrate the calculated time-series behavior of these two factors over the representative multi-day measurement period. The analysis reveals a maximum winding eddy-current loss factor F_{HL} of 42.9 and a maximum other stray loss factor $F_{HL\text{-}STR}$ of 3.89.

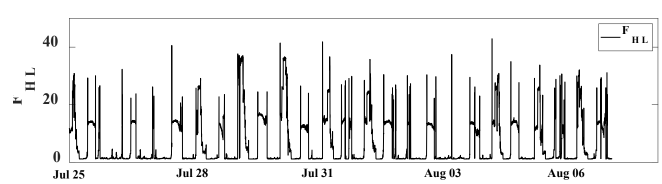

Figure 8. Harmonic loss factor for winding eddy currents over time.

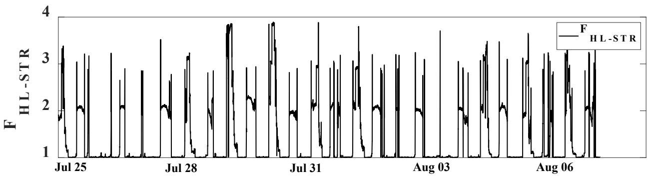

Figure 9. Harmonic loss factor for other stray losses over time.

However, the assessment reveals an inverse relationship between the loss factors and the load conditions. The peak values for both factors are found to occur during low-load or intermittent charging periods. This behavior is identified as an artifact of the calculation at very low (near-zero) fundamental current, similar to the inflation observed in THD_i. As the load increases, the harmonic loss factors decrease from these extreme peaks and settle into a more stable range. During these high-load periods (i.e., the early morning peak), the factor F_{HL} is consistently observed fluctuating between 10 and 30.

To statistically summarize the distribution of these harmonic loss factors over the shown period, the box plot is presented in Fig. 10. The plot for F_{HL} shows a median value of 1.4 but with a wide interquartile range and significant outliers. In contrast, the $F_{HL\text{-}STR}$ plot is tightly clustered below 2.5.

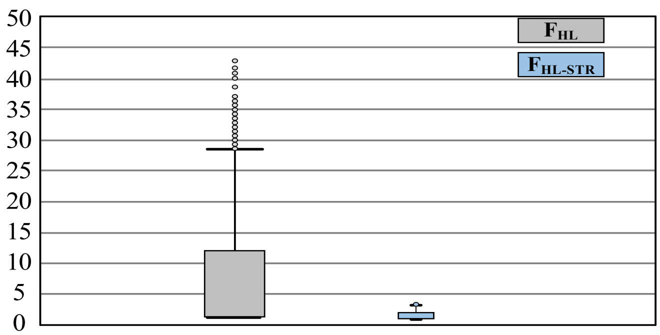

Figure 10. Box plot statistical summary of two harmonic loss factors.

Interpreting harmonic loss factors alone obscures the true severity of the power quality impact. To quantify the actual threat to asset health, the I_{max} is calculated using (7). The minimum I_{max} observed over the entire measurement period is 0.83 p.u. This reveals that the transformer's effective capacity is derated to 83% under the 46% loading condition. Furthermore, projections indicate that as the station scales towards full utilization, the available capacity could further drop to 70% or lower.

Fig. 11 superimposes the total transformer losses against the TDD. This reveals the spikes in TDD align with the peaks in total power losses, indicating a compounding thermal stress on the transformer.

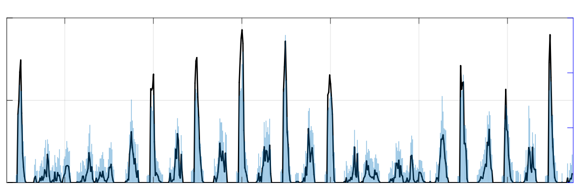

Figure 11. The total transformer losses and TDD over the measurement period.

V. Conclusion

This paper presents a field-based assessment of harmonic-induced losses in an electric bus charging station. By integrating empirical measurements with the analytical framework of IEEE Std. C57.110, the study provides a validated quantification of harmonic impacts in a real-world environment. One key contribution of this work is the identification of metric inflation in variable-load settings, where indices like THD_i yield extreme values during low-load periods. For practical implementation, it is recommended that the monitoring strategy prioritizes TDD to accurately reflect the true harmonic impacts during peak loading conditions.

The study quantifies the actual impact on asset longevity through the I_{max}, revealing that the transformer is derated to 83% of its capacity. Although the current 46% loading remains within safe limits, the analysis exposes a compounding thermal stress, where peak harmonic injection occurs synchronously with maximum operational losses. Projections indicate that as the station scales toward full utilization, the effective capacity could further decline to 70% or lower. This empirical finding confirms that the application of harmonic derating factors is not merely a theoretical precaution. Rather, it is an essential requirement for reliable asset management and future design of large-scale EV charging infrastructure.

References

[1] Y. Iscanoglu and M. Yilmaz, "Cost-effective electrification of city BRT systems: Optimizing battery and charging infrastructure for sustainable urban mobility," *IEEE Access*, vol. 12, pp. 187220-187233, Dec. 2024.

[2] L. Wang, Z. Qin, T. Slangen, P. Bauer, and T. V. Wijk, "Grid impact of electric vehicle fast charging stations: Trends, standards, issues, and mitigation measures – An overview," *IEEE Open J. Power Electron*., vol. 2, pp. 56-74, Jan. 2021.

[3] P. Rodríguez-Pajarón, A. Hernández, and J. V. Milanović, "Probabilistic assessment of the impact of electric vehicles and nonlinear loads on power quality in residential networks," *Int. J. Electr. Power Energy Syst*., vol. 129, Jul. 2021, Art. no. 106807.

[4] *IEEE Standard for Harmonic Control in Electric Power Systems*, IEEE Standard 519, Aug. 2022.

[5] Y. Shi, Z. Tang, H. Li, S. Wu, and H. Wang, "Impact of harmonic distortions due to scaled EV charging in residential distribution cable systems considering the filtering effect of distribution cable π model," *IEEE Access*, vol. 13, pp. 51499-51512, Mar. 2025.

[6] L. M. Caro, G. Ramos, K. Rauma, D. F. C. Rodriguez, D. M. Martinez, and C. Rehtanz, "State of charge influence on the harmonic distortion from electric vehicle," *IEEE Trans. Ind. Appl.*, vol. 57, no. 3, pp. 2077-2088, May-Jun. 2021.

[7] A. Ahmed, A. Iqbal, I. Khan, A. Al-Wahedi, H. Mehrjerdi, and S. Rahman, "Impact of EV charging station penetration on harmonic distortion level in utility distribution network: A case study of Qatar," in *Proc. IEEE Texas Power Energy Conf*., Feb. 2021, pp. 1-6.

[8] *IEEE Recommended Practice for Establishing Liquid-Immersed and Dry-Type Power and Distribution Transformer Capability When Supplying Nonsinusoidal Load Currents*, IEEE Std. C57.110™-2018, pp. 1-68, Oct. 2018.

[9] K. D. McBee and M. G. Simões, "General smart meter guidelines to accurately assess the aging of distribution transformers," *IEEE Trans. Smart Grid*, vol. 5, no. 6, pp. 2967-2979, Nov. 2014.

[10] D. Pejovovski, K. Najdenkoski, and M. Digalovski, "Impact of different harmonic loads on distribution transformers," *Proc. Eng*., vol. 202, pp. 76-87, Jan. 2017.

[11] L. H. Dixon, "Eddy current loss in transformer windings and circuit wiring," Texas Instruments, 2003.

[12] M. A. Taher, S. Kamel, and Z. M. Ali, "K-Factor and transformer losses calculations under harmonics," in *Proc. 18th Int. Middle East Power Syst. Conf.* (*MEPCON*), Cairo, Egypt, pp. 1-6, Dec. 2016.